Available online at www.sciencedirect.com
SCIENCE DIRECT®
Journal of Solid State Chemistry 178 (2005) 847–854
JOURNAL OF SOLID STATE CHEMISTRY
www.elsevier.com/locate/jssc

Structural refinement of $Nd[Fe(CN)_6]\cdot 4H_2O$ and study of $NdFeO_3$ obtained by its oxidative thermal decomposition at very low temperatures

M. Carolina Navarro[a], Elisa V. Pannunzio-Miner[b], Silvina Pagola[b], M. Inés Gómez[a], Raúl E. Carbonio[b,*]

[a]*Instituto de Química Inorgánica, Facultad de Bioquímica, Química y Farmacia, Universidad Nacional de Tucumán, Ayacucho 491, 4000 San Miguel de Tucumán, Argentina*

[b]*Departamento de Fisicoquímica, Facultad de Ciencias Químicas, Instituto de Investigaciones en Físico Química de Córdoba (INFIQC), Universidad Nacional de Córdoba. Ciudad Universitaria, 5000 Córdoba, Argentina*

Received 13 August 2004; received in revised form 1 November 2004; accepted 15 November 2004

Abstract

The crystal structure of $Nd[Fe(CN)_6]\cdot 4H_2O$ has been refined by Rietveld analysis using high resolution synchrotron powder X-ray diffraction data. It belonged to the orthorhombic crystal system, *Cmcm* space group, with cell parameters: $a = 7.473952(1)$ Å, $b = 12.919104(2)$ Å and $c = 13.800549(2)$ Å. The change in space group from $P6_3/m$ which is observed in the pentahydrates ($LnFe(CN)_6\cdot 5H_2O$) to *Cmcm* in the tetrahydrates has been analyzed to be a consequence of the change in 9-fold coordination of Nd^{3+} in the pentahydrates to 8-fold coordination in the tetrahydrates, which changes the Nd^{3+} environment from tricapped trigonal prism to a distorted tricapped trigonal prism or square antiprism. Its decomposition process in air to produce $NdFeO_3$ has been followed by thermogravimetric and differential thermal analysis, IR spectroscopy and laboratory powder XRD. We found that it is possible to synthesize crystalline $NdFeO_3$ at temperatures as low as 380 °C and refine the structure of single phase crystalline $NdFeO_3$ synthesized by this method at 600 °C.

Keywords: $Nd[Fe(CN)_6]\cdot 4H_2O$; Structure refinement; Synchrotron X-ray diffraction; $NdFeO_3$; Low temperature synthesis

1. Introduction

Heteronuclear complexes of the type $LnM'L_n\cdot nH_2O$, $LnM'_xM''_{1-x}L_n\cdot zH_2O$ or (Ln, A)$M'L_n\cdot zH_2O$ (where Ln is a lanthanide, A is an alkaline earth metal, M′ and M″ are transition metals and L is a ligand) have been extensively studied as precursors for the low temperature synthesis of high surface area perovskite-type oxides $LnMO_3$, $LnM'_xM''_{1-x}O_3$ and (Ln, A)$M'O_3$, respectively [1–17]. This method was first proposed by Gallagher in 1968 [5]. The mixing of metal cations at the atomic level and with the desired stoichiometry of the metals in the heteronuclear complex allows lowering the synthesis temperature down to the range 600–800 °C, well below the usual temperatures used in the conventional ceramic method, thus avoiding the sintering of the material and producing high surface area and homogeneous materials. Because powders with excellent properties to use in screen-printing are produced, this method is preferred for the preparation of homogeneous thick films for sensor applications [3,9–11,16,17]. Perovskite-type oxides are also extensively used as catalyst for a number of applications, i.e., as tree-way catalysts [18], methane flameless combustion [19], NO reduction by CO [20] and catalytic destruction of VOCs [21] among others. Despite the potentiality of the heteronuclear complexes decomposition method to produce

*Corresponding author. Fax: +54 351 433 4188.
E-mail address: carbonio@mail.fcq.unc.edu.ar (R.E. Carbonio).

0022-4596/$ - see front matter © 2004 Elsevier Inc. All rights reserved.
doi:10.1016/j.jssc.2004.11.026

homogeneous high surface area materials, few publications reported its use for catalysts preparation [12,13]. Some of us have used alkaline earth nitroprussides ($AFe[(CN)_5NO]\cdot nH_2O$) to prepare high surface area $AFeO_{3-\delta}$ perovskites [14,15] in the temperature range 700–900 °C with a high Fe(IV) content. Moreover, we have prepared a new polytype in the system $BaFeO_{3-\delta}$, $BaFeO_{2.8-\delta}$ [15], and solved its structure ab initio from high resolution synchrotron powder X-ray diffraction.

Lanthanide hexacianometallates are among the most used heteronuclear complexes for perovskite oxide synthesis [1–4,6,7–9,11,16,17], thus, the study of their structures and decomposition processes is very important to understand the synthesis of homogeneous perovskite-type oxides materials at low temperatures.

Among the lanthanide hexacianometallates, the lanthanide hexacyanoferrates (III) *n*-hydrates ($Ln[Fe(CN)_6]\cdot nH_2O$) have been extensively studied [22–33]. The large lanthanide ions (La, Ce and Pr) form the hexagonal pentahydrate ($Ln[Fe(CN)_6]\cdot 5H_2O$), belonging to the space group $P6_3/m$, while the smaller ones (Sm ~Yb) form the tetrahydrate ($Ln[Fe(CN)_6]\cdot 4H_2O$) with the space group *Cmcm*. Masuda and co-workers [31,32] have found that the boundary complex is the neodimium compound ($Nd[Fe(CN)_6]\cdot nH_2O$), where the *n* value can change reversibly from 4 (space group *Cmcm*) to 5 (space group $P6_3/m$). The large value of the equivalent isotropic thermal parameter ($B_{eq} = 12\,\text{Å}^2$) for the three O(1) corresponding to coordinated water molecules guide them to the conclusion that these molecules are vigorously moving and one of them seems to easily dissociate. The structure of the pentahydrate has been refined by them [31], however, even if they mention that the tetrahydrate is isostructural with other tetrahydrates of lanthanide hexacianoferrates, its structure has not been refined up to now.

Detailed studies of the decomposition process for $Ln[Fe(CN)_6]\cdot nH_2O$ have been made by Sadaoka and co-workers [2,4,6]. They found that after calcinations for 30 min [4] or 1 h [2] they could obtain a single perovskite phase at temperatures between 620 and 830 °C, depending on the lanthanide, increasing the minimum temperature as the ionic radii of the lanthanide decreases. They also found that it was possible to obtain single phase $LaFeO_3$ by increasing the time up to 100 h at a temperature of 350 °C, but did not make the same study for $NdFeO_3$.

In the present paper we refine the structure of $Nd[Fe(CN)_6]\cdot 4H_2O$ using high resolution synchrotron X-ray powder diffraction (SXRPD). We also study the decomposition process to produce $NdFeO_3$ using IR, thermogravimetric and differential thermal analysis (TGA and DTA) and laboratory powder XRD and refine the structure of $NdFeO_3$ obtained at temperatures between 380 and 600 °C.

2. Experimental

$Nd[Fe(CN)_6]\cdot 4H_2O$ was prepared by mixing equal volumes of 1 M $K_3[Fe(CN)_6]$ and 1 M $Nd(NO_3)_3\cdot 6H_2O$, stirred during two hours, filtered and thoroughly washed with water, ethanol and ethyl ether and finally stored in a dry box with silica gel.

IR spectroscopy, thermogravimmetric analysis (TGA), and powder XRD were used to follow the decomposition process. IR spectra were recorded with an FTIR Perkin Elmer 1600 in the transmission mode using KBr pellets. Thermogravimetric and DTA measurements were performed in a Shimadzu TGA/DTA 50 at 5 °C/min under flowing air. Laboratory powder XRD experiments for samples prepared at 320, 380 and 400 °C were performed with a Rigaku Miniflex diffractometer with Cu$K\alpha$ radiation ($\lambda = 1.5418$ Å) between 20° and 90° in 2θ, steps of 0.02° and counting time of 4 s. Laboratory powder XRD pattern for the sample prepared at 600 °C was taken in a Philips PW1710 diffractometer, with Cu$K\alpha$ radiation ($\lambda = 1.5418$ Å) between 20° and 90° in 2θ, steps of 0.02° and counting time of 5 s. Rietveld structure refinements of $NdFeO_3$ samples were performed using the FULLPROF program [34], with laboratory powder XRD data, in the space group *Pnma*, with the initial structural model informed in Ref. [35]. For the samples prepared at 380 and 400 °C, only profile parameters, overall isotropic temperature factor, cell parameters and scale factor were refined. Atomic positions were fixed to the values obtained from the initial model because the diffraction patterns were not of enough quality. For the sample prepared at 600 °C, atomic positions and isotropic temperature factors were also refined.

The high resolution SXRPD data for the structural refinement of $Nd[Fe(CN)_6]\cdot 4H_2O$ were collected at room temperature at the SUNY X3B1 powder diffraction beamline of NSLS, Brookhaven National Laboratory. The wavelength (0.700016 Å) was selected by a monochromator consisting of two parallel Si(111) crystals. The incident beam was monitored by an ion chamber. The out-of-plane resolution in the diffracted beam was given by slits whereas the in-plane resolution was determined by a Ge(111) analyzer crystal. The diffracted beam was measured with an NaI(Tl) scintillation detector. The sample was rocked about the diving portion in a zero-background quartz sample holder. Data were collected between 2.000° and 40.016° in 2θ with a step size of 0.003° and a counting time of 1 s per step. Rietveld structure refinement was also performed using the FULLPROF program, in the space group *Cmcm* using as initial model the structure of $Gd[Fe(CN)_6]\cdot 4H_2O$ [33]. A pseudo-Voigt function convoluted with an axial divergence asymmetry function [36] was chosen to generate the peak shapes. The background intensities were subtracted as the linear

interpolation between 23 given points. No regions were excluded and the following parameters were refined: zero-point, scale factor, pseudo-Voigt parameters of the peak shape, full-width at half-maximum, positional, anisotropic thermal and cell parameters. In the final refinement cycles, the shifts in the atomic parameters were zero up to the fourth decimal figure.

3. Results and discussion

3.1. $Nd[Fe(CN)_6]\cdot 4H_2O$

3.1.1. Structural refinement

The refined SXRPD data at RT are shown in Fig. 1. No impurities were observed in the pattern. Final cell parameters, atomic positions, anisotropic thermal factors (except for C2) and discrepancy parameters are shown in Table 1. Anisotropic thermal factors for C2 could not be refined because some β_{nn} values went negative. Some selected interatomic distances are shown in Table 2. A view of the structure is shown in Fig. 2. As recently discussed by Masuda and co-workers [31,32], the pentahydrate transforms in the tetrahydrate by loosing one of the waters coordinated to Ln^{3+} ions, so that its coordination number changes from 9 to 8. As can be seen in Table 2, Nd^{3+} is coordinated to four N(1), two N(2) and two O(1) forming a bicapped (distorted) trigonal prism coordination (Fig. 3b) like other large 8-fold coordinated cations, i.e. Ca^{2+} in $CaFe_2O_4$ [37] and Sr^{2+} in $Sr(OH)_2\cdot H_2O$ [38]. Fe^{3+} is

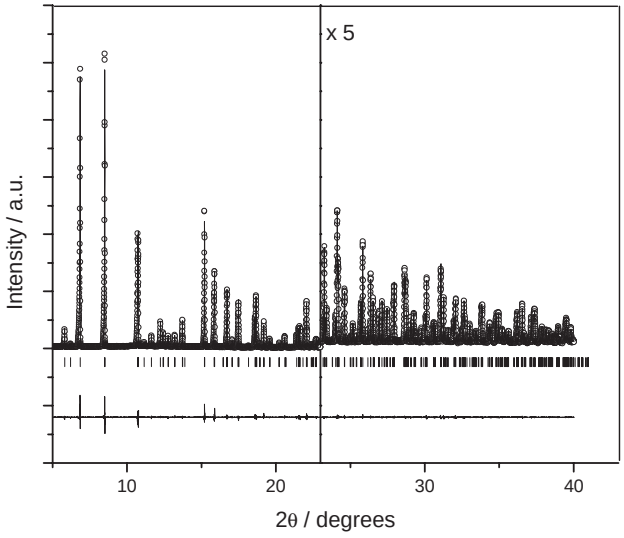

Fig. 1. SXRPD taken at room temperature for $Nd[Fe(CN)_6]\cdot 4H_2O$, refined in the space group *Cmcm*. Observed (circles), calculated (solid line) and difference (at the bottom). Zooming ($\times 5$) for $2\theta > 23^\circ$ is shown. Vertical marks correspond to the position of the allowed Bragg reflections.

Table 2
Some selected Interatomic distances (Å) and angles (deg) with e.s.d. 's in parentheses (See Fig. 2(b) for bonds identification)

(Nd)–(N)			
(Nd)–(N1)	2.545(5) ×4	N(1)–Nd–N(1)	117.540(310)
(Nd)–(N2)	2.553(7) ×2	N(2)–Nd–N(2)	112.456(485)
<(Nd)–(N)>	2.548(6)	N(1)–Nd–N(2)	77.298(313)
		N(1)–Nd–N(2)	142.779(430)
(Nd)–(O)			
(Nd)–(O1)	2.446(5) ×2	O(1)–Nd–O(1)	109.206(298)
		O(1)–Nd–N(1)	79.215(263)
		O(1)–Nd–N(1)	141.977(343)
		O(1)–Nd–N(2)	71.217(273)
(Fe)–(C)			
(Fe)–(C1)	1.878(6) ×4	C(1)–Fe–C(1)	86.4(4)
(Fe)–(C2)	1.940(9) ×2	C(1)–Fe–C(1)	180.0(6)
<(Fe)–(C)>	1.899(7)	C(1)–Fe–C(1)	93.5(5)
		C(1)–Fe–C(2)	89.1(6)
(C)–(N)		C(1)–Fe–C(2)	91.0(6)
(C1)–(N1)	1.190(8) ×3	C(2)–Fe–C(2)	180.0(9)
(C2)–(N2)	1.125(1) ×3		
<(C)–(N)>	1.157(4)		
(O1)…(O2)	2.8429(45)		

Table 1
Crystallographic parameters for $Nd[Fe(CN)_6]\cdot 4H_2O$ after Rietveld refinement[a] of synchrotron powder XRD data at 298 K

Atom	Wyckoff site	x	y	z	Anisotropic temperature factors					
					$\beta_{11}\times 10^4$	$\beta_{22}\times 10^4$	$\beta_{33}\times 10^4$	$\beta_{12}\times 10^4$	$\beta_{13}\times 10^4$	$\beta_{32}\times 10^4$
Nd	4*c*	0	0.32364(6)	0.25	16(1)	20.0(6)	9.8(4)	0	0	0
Fe	4*a*	0	0	0	7(4)	21(1)	7.9(9)	0	0	2(1)
C1	16*h*	0.3169(9)	0.4561(5)	0.0836(4)	160(20)	11(6)	18(5)	−1(8)	−34(8)	−5(5)
C2[b]	8*f*	0	0.1334(7)	0.0647(7)	—	—	—	—	—	—
N1	16*h*	0.2036(6)	0.4257(4)	0.1372(3)	130(20)	30(4)	6(4)	8(7)	16(5)	4(4)
N2	8*f*	0	0.2137(5)	0.0962(5)	100(20)	26(7)	42(7)	0	0	18(5)
O1	8*g*	0.2670(6)	0.2140(4)	0.25	170(20)	58(6)	45(4)	60(7)	0	0
O2	8*f*	0	0.6535(5)	0.0973(3)	100(10)	66(6)	45(3)	0	0	−18(5)

Space group: *Cmcm* (No. 63), cell parameters: $a = 7.473952(1)$ Å, $b = 12.919104(2)$ Å, $c = 13.800549(2)$ Å, Vol = 1332.536(4) Å^3, $Z = 4$.
[a]Discrepance parameters: $R_{wp} = 9.28$, $R_{exp} = 5.16$, $\chi^2 = 3.23$, $R_{Bragg} = 2.21$, $R_p = 8.39$.
[b]Isotropic temperature factor for C2: 0.7(2) Å^2.

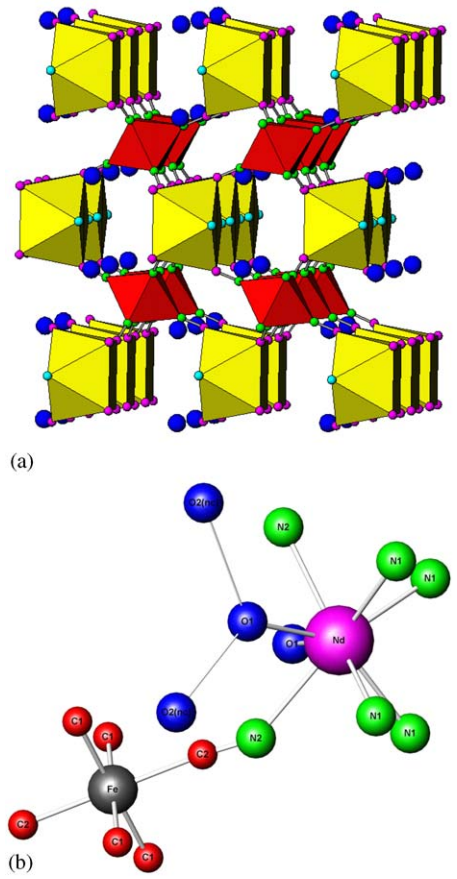

Fig. 2. (a) View of the structure of $Nd[Fe(CN)_6]\cdot 4H_2O$ along the [100] direction (slightly rotated) showing the linkage of polyhedra. Yellow square antiprism: $Nd(N_6O_2)$. Red octahedra: FeC_6. Small light blue spheres: O from coordinated water. Small pink spheres: N. Small green spheres: C. Large blue spheres: O from non-coordinated water. C–N bonds are indicated by thin gray lines. (b) View of the structure of $Nd[Fe(CN)_6]\cdot 4H_2O$ showing coordination around Nd and Fe. O_2 from non-coordinated water is indicated as O_2(nc). Hydrogen bond between coordinated water and non-coordinated water is indicated by a thinner line.

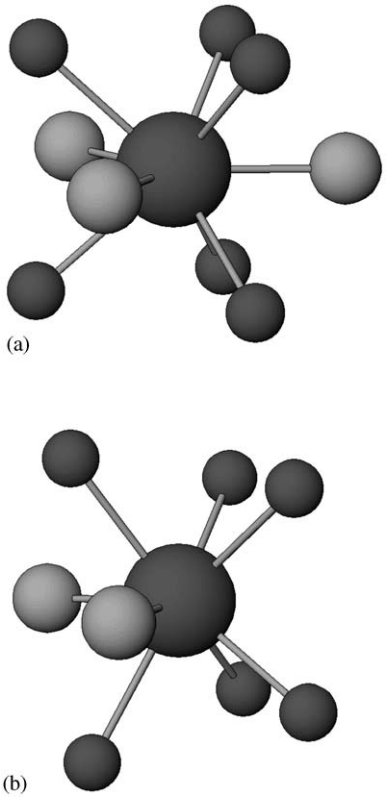

Fig. 3. Coordination polyhedra around Nd in: (a) Tricapped trigonal prism 9-fold coordination for Nd in $Nd[Fe(CN)_6]\cdot 5H_2O$ (Data obtained from reference 31); (b) Bicapped (distorted) trigonal prism 8-fold coordination for Nd in $Nd[Fe(CN)_6]\cdot 4H_2O$ (calculated from data obtained in this paper). Small dark spheres are N atoms and large clear spheres are O atoms.

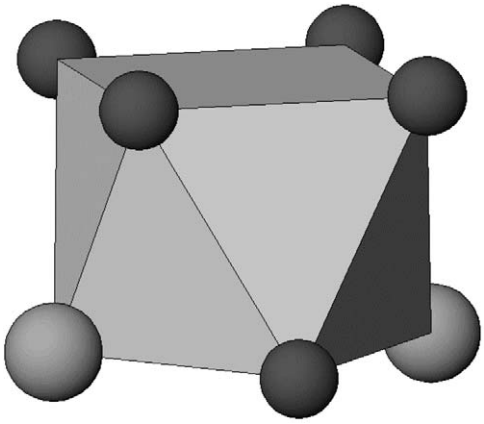

Fig. 4. Nd 8-fold coordination viewed as a square antiprism. Small dark spheres are N atoms and large clear spheres are O atoms.

coordinated to four C(1) and two C(2) with the usual irregular octahedral coordination. Bicapped trigonal prisms $Nd(N_6O_2)$ and irregular octahedra FeC_6 are bridged through CN groups (Fig. 2). The two additional O(2) atoms belong to the two non-coordinated water molecules, which are hydrogen bonded to the coordinated water molecules (d O(1)…O(2) = 2.843(4) Å). The coordination of Ln^{3+} ions in the tetrahydrates (LnN_6O_2) was erroneously assigned as octahedral [30]. This "distorted" bicapped trigonal prism, can be seen, as was previously mentioned by Mullica and Sappenfield [26] as a square antiprism (Fig. 4), however we maintain here the term "distorted" bicapped trigonal prism, in order to make the comparison with the pentahydrates.

In the pentahydrate $Nd[Fe(CN)_6]\cdot 5H_2O$ (36), Nd^{3+} is 9-fold coordinated by a tricapped trigonal prism, a regular trigonal prism NdN_6 with six equivalent Nd–N bonds (d Nd–N = 2.54(1) Å) and three additional identical bonds with O(1) (d Nd–O(1) = 2.42(2) Å) to form the tricapped trigonal prism (Fig. 3a). It is easy to understand the change from pentahydrates to tetrahydrates. As the ionic radii of the Ln^{3+} decreases, one of the coordinated water molecules is loosed to form the

bicapped (distorted) trigonal prism, since it gets more stable to accommodate 8 ligands instead of 9 in the smaller lanthanides. This bicapped (distorted) trigonal prism is distorted as a consequence of the imbalance in repulsions produced by the absence of one of the oxygens.

In the pentahydrate, Nd^{3+} is located in the Wyckoff site 2*d* of the space group $P6_3/m$ with site symmetry −6. The distortion of the trigonal prism NdN_6 (in the tetrahydrate there are two larger Nd–N(2) distances and four shorter Nd–N(1) ones (Table 2) makes the −6 axes to disappear, and to change symmetry from hexagonal (space group $P6_3/m$) to orthorhombic (space group *Cmcm*). In the pentahydrate, Nd^{3+} is located in the Wyckoff site 4*c* of the space group *Cmcm* with a site symmetry *m*2*m*, consistent with the square antiprism 8-fold coordination (Fig. 4).

3.1.2. IR spectra

In order to characterize the complex and their decomposition products IR spectra were recorded in transmission mode. The results for the complex are shown in Fig. 5. Antisymmetric and symmetric *ν*(CN) stretching bands are observed at 2146 and 2135 cm^{-1}, respectively, and *δ*(HOH) bands in the range 1610–1630 cm^{-1}. A sharp *ν*(OH) stretching band is observed at 3622 cm^{-1} and a broad *ν*(OH, hydrogen bonded) stretching band is observed in the range 3000–3570 cm^{-1}. The bands at 2340–2360 correspond to residual CO_2.

3.1.3. Thermogravimetric (TGA) and differential thermal analysis (DTA) data

TGA and DTA data for $Nd[Fe(CN)_6]\cdot 4H_2O$ are shown in Figs. 6 and 7. Three main steps are observed in the TGA (Fig. 6) for the decomposition process in air. The first one which ends at ~280 °C, with a weight loss of 17.11% corresponds to the dehydration process to obtain the anhydrate (theoretical value 16.8%). This corresponds to the endothermic process observed at the same temperature range in the DTA (Fig. 7). The second step in the TGA, which finishes at ~320 °C, has a weight loss of 16.45%. If one assumes that this weight loss corresponds only to loss of CN groups it would give 2.7 CN groups. However, if we consider the extremely large exothermic process (Fig. 7) centered at the same temperature than the second step in the TGA, it is clear that this process corresponds to the combustion of all the CN groups, but part of the CO_2 formed in this combustion clearly gets adsorbed on the surface of the particles as CO_3^{2-}, in this way, we cannot observe the weight loss corresponding to 6 CN groups.

The third step has a weight loss of 8.6% and corresponds to the simultaneous loss of the surface CO_3^{2-} and O_2 uptake to generate the $NdFeO_3$ mixed

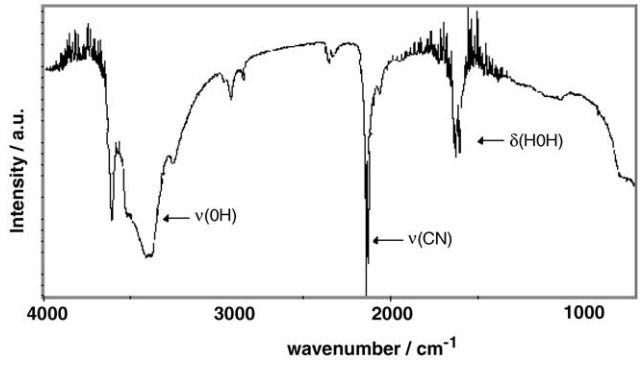

Fig. 5. IR spectra for $Nd[Fe(CN)_6]\cdot 4H_2O$.

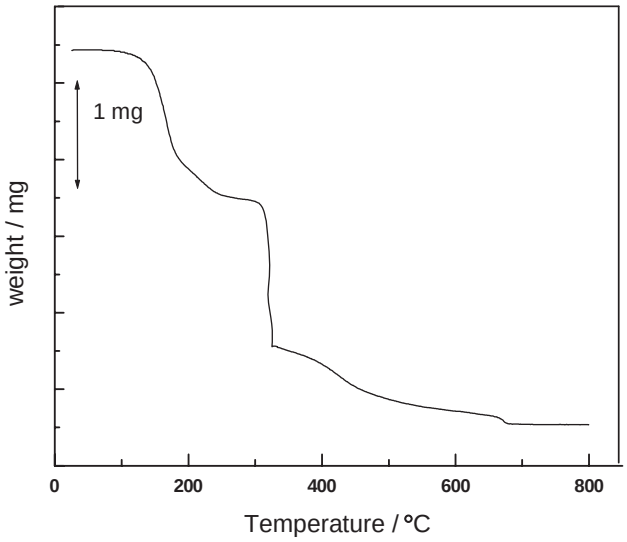

Fig. 6. TGA data for $Nd[Fe(CN)_6]\cdot 4H_2O$, taken at 5 °C/min under flowing air.

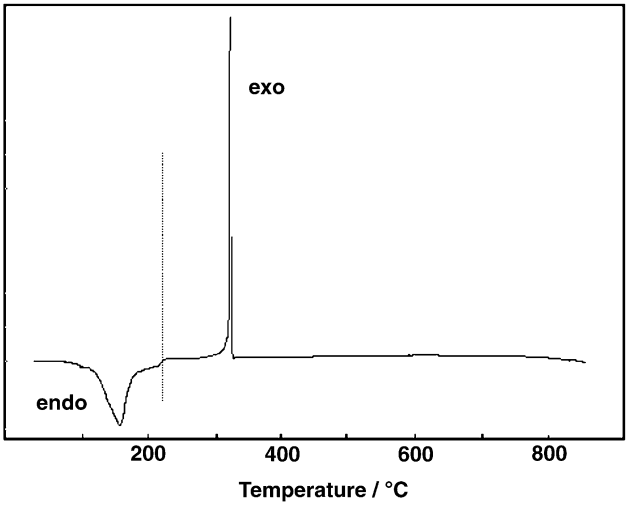

Fig. 7. DTA data for $Nd[Fe(CN)_6]\cdot 4H_2O$, taken at 5 °C/min under flowing air. Zooming (× 30) for T < 200 °C is shown.

oxide. The total weight loss from room temperature to ~ 700 °C (42.1%) corresponds exactly with the total reaction:

$$Nd[Fe(CN)_6]\cdot 4H_2O + 7.5O_2 \rightarrow NdFeO_3 + 6CO_2 + 3N_2 + 4H_2O$$

We will not speculate about the decomposition mechanism, since this is not the objective of this paper.

3.2. $NdFeO_3$ obtained by heat treatment of $Nd[Fe(CN)_6]\cdot 4H_2O$ at different temperatures

3.2.1. Laboratory powder XRD and IR spectra

Laboratory powder XRD data obtained at room temperature for $NdFeO_3$ samples prepared by heat treatment of $Nd[Fe(CN)_6]\cdot 4H_2O$ in air during 72 h at different temperatures are shown in Fig. 8. A broad peak centered at ca. 32° in 2θ is observed at the lower temperatures (320 and 350 °C). This was previously observed by Sadaoka et al. [2,4,6] for samples heat treated during 30–60 min at temperatures lower than 620–830 °C, depending on the lanthanide, increasing the limiting temperature as the ionic radii of the lanthanide decreases. This broad peak was assigned to a vitreous phase, which is formed as an intermediate phase during the synthesis of the perovskite oxide from the complex decomposition.

Here we observe quite well defined XRD patterns for samples heat treated at 380 °C or higher temperatures. Rietveld refinements of powder XRD data obtained at 380 and 400°C (not shown) show good crystallized samples with cell parameters very similar to those informed in literature (Table 3). Rietveld refinement of the sample obtained at 600 °C (Fig. 9) shows a well crystallized single phase.

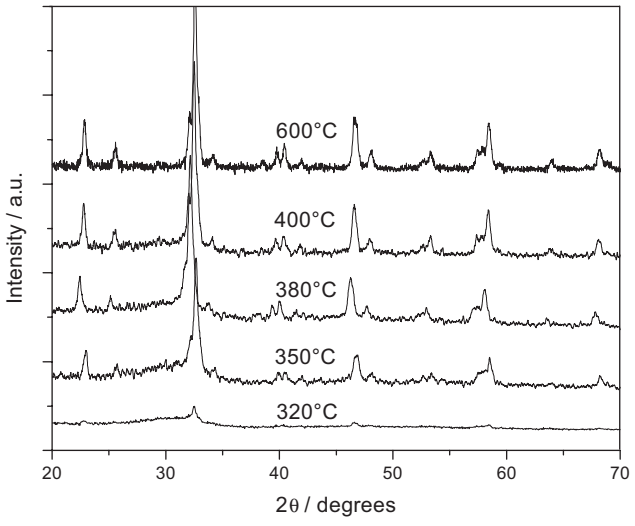

Fig. 8. Laboratory powder X-ray diffractograms taken at room temperature for $NdFeO_3$ samples obtained by heat treatment of $Nd[Fe(CN)_6]\cdot 4H_2O$ in air, during 72 h at different temperatures (their values are indicated in the figure).

Table 3
Refined cell parameters and cell volume for $NdFeO_3$ prepared from the oxidative thermal decomposition of $Nd[Fe(CN)_6]\cdot 4H_2O$ at different temperatures during 72 h

T/°C	a/Å	b/Å	c/Å	Vol/Å^3
380	5.5813(1)	7.7600(1)	5.4487(1)	236.00(1)
400	5.5965(4)	7.7848(5)	5.4580(4)	237.80(3)
600	5.5849(3)	7.7645(5)	5.4521(3)	236.43(2)

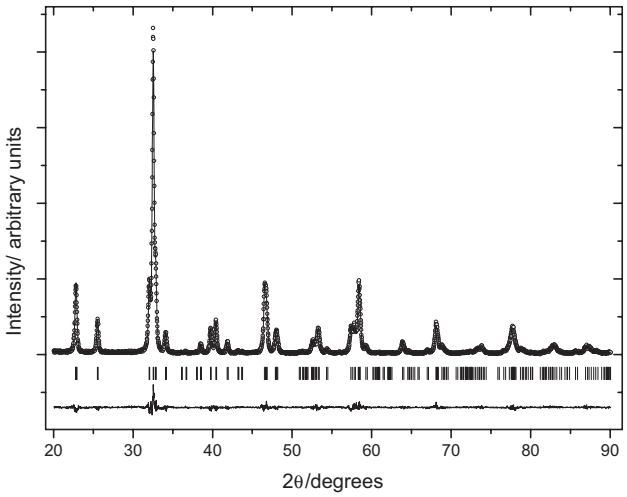

Fig. 9. Laboratory X-ray powder difractogram taken at room temperature for $NdFeO_3$ refined in the space group *Pnma*. Observed (circles), calculated (solid line) and difference (at the bottom). Vertical marks correspond to the position of the allowed Bragg reflections. Sample obtained by heat treatment of $Nd[Fe(CN)_6]\cdot 4H_2O$ in air at 600 °C during 72 h.

Table 4
Crystallographic parameters for $NdFeO_3$ synthesized from the oxidative thermal decomposition of $Nd[Fe(CN)_6]\cdot 4H_2O$ at 600 °C during 72 h, after Rietveld refinement[a] of laboratory powder XRD data at 298 K

Atom	Wyckoff site	x	y	z	B_{iso}
Nd	4*c*	0.04783(1)	0.25	−0.01100(3)	0.319(3)
Fe	4*b*	0	0	0	0.031(5)
O1	4*c*	0.4721(2)	0.25	0.0845(3)	1.79(3)
O2	8*d*	−0.2941(1)	−0.0462(1)	0.2940(2)	1.36(2)

Space group: *Pnma* (No. 62), cell parameters: $a = 5.5849(3)$ Å, $b = 7.7645(5)$ Å, $c = 5.4521(3)$ Å, Vol = 236.43(2) Å^3, $Z = 4$.
[a]Discrepancy parameters: $R_{wp} = 12.4$; $R_{exp} = 11.17$; $\chi^2 = 1.24$; $R_{Bragg} = 2.74$; $R_p = 8.85$.

Results for the complete structural refinement for $NdFeO_3$ prepared at 600 °C are shown in Table 4. Our results are in good agreement with the structural

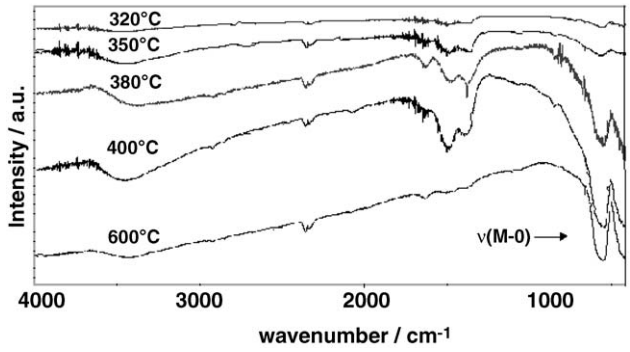

Fig. 10. IR spectra for $NdFeO_3$ samples obtained by heat treatment of $Nd[Fe(CN)_6]\cdot 4H_2O$ in air, during 72 h at different temperatures (their values are indicated in the figure).

refinement made from single crystal data reported in the literature [35].

IR spectra obtained for the same samples are shown in Fig. 10. ν(CN) stretching bands could not be observed in any of the samples. Bands corresponding to CO_3^{2-} are observed in the range 1300–1450 and at 840 cm^{-1}, for all the samples, decreasing its intensity as heat temperature increases. Even in the sample prepared at 600 °C the bands in the range 1300–1450 cm^{-1} could be observed. The broadband observed in the range 3200–3700 cm^{-1} is attributed to surface-adsorbed −OH species. Since carbonates could not be detected by powder XRD, we attribute their bands also to surface-adsorbed species, which is reasonable since these are high surface materials. This is in agreement with the observation made by Sadaoka et al. [4] in the sense that the surface of particles obtained by decomposition of lanthanide hexacianoferrates are very active to chemisorption of CO_2 and the consequent carbonate formation on the surface. We have found similar results for $AFeO_{3-\delta}$ (A = Ca, Sr) prepared from the oxidative thermal decomposition of $A[Fe(CN)_5NO]\cdot 4H_2O$ [14].

ν(MO) stretching bands corresponding to $NdFeO_3$ are observed in the 430–700 range. This are insinuated as small bands in the samples prepared at 320 and 350 °C, but are strong bands in the samples prepared at 380, 400 and 600 °C, which agrees with the observation made through powder XRD that the perovskite has already been formed as a single crystalline phase at temperatures of 380 °C or higher.

4. Conclusions

We have refined the structure of $Nd[Fe(CN)_6]\cdot 4H_2O$ by Rietveld analysis using high resolution synchrotron powder diffraction data. The compound crystallizes in the orthorhombic crystal system, space group *Cmcm*, cell parameters: $a = 7.473952(1)$ Å, $b = 12.919104(2)$ Å and $c = 13.800549(2)$ Å. In this structure Nd coordination is 8-fold with a bicapped "distorted" trigonal prism geometry, $Nd(N_6O_2)$. We compare this structure with the one of the pentahydrate ($Nd[Fe(CN)_6]\cdot 5H_2O$), which crystallizes in the hexagonal system, space group $P6_3/m$. The Nd coordination in this structure is 9-fold, with a regular tricapped trigonal prism geometry, $Nd(N_6O_3)$. In the dehydration process when going from the pentahydrate to the tetrahydrate, one coordinated water is lossed, and the regular tricapped trigonal prism geometry, $Nd(N_6O_3)$, transforms into a bicapped "distorted" trigonal prism geometry, $Nd(N_6O_2)$. This distortion can be explained by the imbalance in repulsions produced by the absence of one of the oxygens. Actually, this bicapped "distorted" trigonal prism, can be better understood as a square antiprism with the oxygens in trans positions. The change in space group from $P6_3/m$ in the pentahydrates to *Cmcm* in the tetrahydrates can be explained because in the pentahydrate, Nd^{3+} is located in the Wyckoff site 2*d* of the space group $P6_3/m$ with site symmetry −6. The distortion of the trigonal prism NdN_6 makes the −6 axes to disappear, and to change symmetry from hexagonal (space group $P6_3/m$) to orthorhombic (space group *Cmcm*). In the pentahydrate, Nd^{3+} is located in the Wyckoff site 4*c* of the space group *Cmcm* with a site symmetry *m*2*m*, consistent with the square antiprism 8-fold coordination.

We could prepare crystalline $NdFeO_3$ at temperatures as low as 380 °C, by the oxidative thermal decomposition of $Nd[Fe(CN)_6]\cdot 4H_2O$, by increasing the heating time up to 72 h. We obtain crystalline single phase $NdFeO_3$ at 600 °C and refine its structure by Rietveld analysis. IR spectroscopy show that samples prepared at 380 and 400 °C contained surface adsorbed carbonate, which can only be eliminated at 600 °C. We have refined the structure of the single-phase sample obtained at 600 °C by Rietveld analysis of laboratory powder XRD.

Acknowledgments

R.E.C.Thanks ANPCYT (Project PICT 12-5378), SECyT-UNC (Project 194/00), Fundación Antorchas (Project 14116-15) and CONICET, (PIP No. 380/98). E. V. Pannunzio-Miner and M.C. Navarro thank CONICET for their fellowships. M.I.G. and M.C.N. thank CIUNT for financial support. Part of this research has been performed at the NSLS, Brookhaven National Laboratory, which is supported by the US DOE, Division of Chemical Sciences and Division of Materials Sciences. Part of this work has been supported by US NSF Grant DMR95-01325. The SUNY X3B1 beamline at the National Synchrotron Light Source is supported by the Division of Basic Energy Sciences of the US DOE (DE-FG02-86ER45231).

References

[1] E. Traversa, P. Nunziante, M. Sakamoto, Y. Sadaoka, M.C. Carotta, G. Martinelli, J. Mater. Res. 13 (1998) 1335–1344.
[2] E. Traversa, M. Sakamoto, Y. Sadaoka, Particulate Sci. Technol. 16 (1998) 185–214.
[3] M.C. Carotta, M.A. Butturi, G. Martinelli, Y. Sadaoka, P. Nunziante, E. Traversa, Sensors Actuators B 44 (1997) 590–594.
[4] Y. Sadaoka, K. Watanabe, Y. Sakai, M. Sakamoto, J. Alloys Compd. 224 (1995) 194–198.
[5] P.K. Gallagher, Mater. Res. Bull. 3 (1968) 225–232.
[6] Y. Sadaoka, H. Aono, E. Traversa, M. Sakamoto, J. Alloys Compd. 278 (1998) 135–141.
[7] S. Matsushima, M. Sakamoto, H. Aono, Y. Sadaoka, Solid State Ionics 108 (1998) 31–36.
[8] E. Traversa, P. Nunziante, M. Sakamoto, Y. Sadaoka, R. Montanari, Mater. Res. Bull. 33 (1998) 673–681.
[9] G. Martinelli, M.C. Carotta, M. Ferroni, Y. Sadaoka, E. Traversa, Sensors Actuators B 55 (1999) 99–110.
[10] J. Shi, R. Yan, Y. Zhu, X. Zhang, Talanta 6 (2003) 157–164.
[11] J.W. Yoon, M.L. Grilli, E. Di Bartolomeo, R. Polini, E. Traversa, Sensors Actuators B 76 (2001) 483–488.
[12] A. González, E. Martínez Tamayo, A. Beltrán Porter, V. Cortés Corberán, Catal. Today 33 (1997) 361–369.
[13] Y. Zhu, R. Tan, J. Feng, S. Ji, L. Cao, Appl. Catal. A: General 209 (2001) 71–77.
[14] M.I. Gómez, J.A. de Morán, R.E. Carbonio, P.J. Aymonino, J. Solid State Chem. 142 (1999) 138–145.
[15] M.I. Gómez, G. Lucotti, J.A. de Morán, P.J. Aymonino, S. Pagola, P. Stephens, R.E. Carbonio, J. Solid State Chem. 160 (2001) 17–24.
[16] H. Aono, E. Traversa, M. Sakamoto, Y. Sadaoka, Sensors Actuators B 94 (2003) 132–139.
[17] M. Tomoda, S. Okano, Y. Itagaki, H. Aono, Y. Sadaoka, Sensors Actuators B 97 (2004) 190–197.
[18] H. He, H.X. Dai, C.T. Au, Appl. Catal. B: Environmental 33 (2001) 65–80.
[19] C. Oliva, L. Forni, A. D'Ambrosio, F. Navarrini, A.D. Stepanov, Z.D. Kagramanov, A.I. Mikhailichenko, Appl. Catal. A: General 205 (2001) 245–252.
[20] V.C. Belessi, C.N. Costa, T.V. Bakas, T. Anastasiadou, P.J. Pomonis, A.M. Efstathiou, Catal. Today 59 (2000) 347–363.
[21] G. Sinquin, C. Petit, S. Libs, J.P. Hindermann, A. Kiennemann, Appl. Catal. B: Environmental 27 (2000) 105–115.
[22] D.F. Mullica, E.L. Sappenfield, Acta Crystallogr. C 47 (1991) 2433–2435.
[23] D.F. Mullica, H.O. Perkins, E.L. Sappenfield, J. Solid State Chem. 74 (1988) 419–423.
[24] D.F. Mullica, H.O. Perkins, E.L. Sappenfield, D.A. Grossie, J. Solid State Chem. 74 (1988) 9–15.
[25] W. Setter, V. Gramlich, F. Hullinger, J. Solid State Chem. 82 (1989) 161–167.
[26] D.F. Mullica, E.L. Sappenfield, J. Solid State Chem. 82 (1989) 168–171.
[27] D.F. Mullica, H.O. Perkins, E.L. Sappenfield, D. Leschnitzer, Acta Crystallogr. C 45 (1989) 330–331.
[28] R.E. Marsh, Acta Crystallogr. C 45 (1989) 1270.
[29] A. Doman, H. Vetsch, F. Hullinger, W. Petter, Acta Crystallogr. C 46 (1990) 1992–1994.
[30] V. Gramlich, W. Petter, Acta Crystallogr. C 46 (1990) 724–726.
[31] W. Xiaoyu, Y. Yukawa, Y. Masuda, J. Alloys. Compd. 290 (1999) 85–90.
[32] X. Wang, Y. Yukawa, Y. Masuda, J. Alloys Compd. 316 (2001) 107–112.
[33] D.F. Mullica, E.L. Sappenfield, Acta Crystallogr. C 47 (1991) 2433–2435.
[34] J. Rodríguez-Carbajal, Physica B 192 (1993) 55.
[35] V.A. Streltsov, N. Ishizawa, Acta Crystallogr. B 55 (1999) 1–7.
[36] L.W. Finger, D.E. Cox, A.P. Jephcoat, J. Appl. Crystallogr. 27 (1994) 892.
[37] D.F. Becker, J.S. Kasper, Acta Crystallogr. 10 (1957) 332–337.
[38] P. Kuske, B. Engelen, J. Henning, H.D. Lutz, H. Fuess, D. Gregson, Z. Crystallogr. 183 (1988) 319–325.